Journal of Molecular Graphics and Modelling 28 (2010) 533–539

Contents lists available at ScienceDirect

Journal of Molecular Graphics and Modelling

journal homepage: www.elsevier.com/locate/JMGM

Molecular simulations of ultra-low-energy nitrogen ion bombardment of A-DNA in vacuum

Chanisorn Ngaojampa [a], Piyarat Nimmanpipug [a], Liangdeng Yu [b,c], Somboon Anuntalabhochai [d], Vannajan Sanghiran Lee [a,*]

[a] Computational Simulation and Modeling Laboratory (CSML), Department of Chemistry and Center for Innovation in Chemistry, Faculty of Science, Chiang Mai University, Chiang Mai 50200, Thailand
[b] Plasma and Beam Physics Research Facility (PBP), Department of Physics and Materials Science, Faculty of Science, Chiang Mai University, Chiang Mai 50200, Thailand
[c] Thailand Center of Excellence in Physics, Commission on Higher Education, 328 Si Ayutthaya Road, Bangkok 10400, Thailand
[d] Molecular Biology Laboratory, Department of Biology, Faculty of Science, Chiang Mai University, Chiang Mai 50200, Thailand

ARTICLE INFO

Article history:
Received 21 May 2009
Received in revised form 26 November 2009
Accepted 30 November 2009
Available online 4 December 2009

Keywords:
Molecular dynamics
Monte Carlo
Ion bombardment
A-DNA

ABSTRACT

For investigating mechanisms involved in low-energy ion beam induced mutation, besides experiments using low-energy and low-fluence ions to bombard naked DNA, molecular simulations were carried out as an effort towards the insight in molecular interactions between ions and DNA. In the current study, Monte Carlo (MC) and molecular dynamics (MD) simulations were applied. The results of MC simulations provide some clues about the interaction energies and sites of preference of N-ion bombardment on an A-DNA short duplex strand. MD simulations of a single N-ion moving towards the same DNA strand with different linear velocities corresponding to bombardment energies of 0.1, 1, 10 and 100 eV revealed information about changes in bond lengths and visibly distorted structures of bombarded nucleotides. The simulations demonstrated that ion-bombardment-induced DNA change in structure was not a random but preferential effect.

1. Introduction

Recently, low-energy ion beam biotechnology, emerging as a novel and highly interdisciplinary subject, has rapidly been developed [1]. The technology uses low-energy (an order of 10 keV) heavy ion beam, instead of protons, to bombard biological organisms to induce biological effects. The effects can eventually be applied for mutation breeding and gene transfer with high efficiencies. With impressive successes in ion beam biotechnology applications, investigations on relevant mechanisms have followed up. Basically two interaction effects are involved, namely direct and indirect effects [2]. The direct effect comes from the ions direct interacting DNA to cause displacements of the atoms in DNA and therefore bond breakage. The indirect effect is due to ion-bombardment-induced secondary effects such as emissions of secondary electrons and X-ray, generation of heat and production of radicals, which can also cause DNA structural changes. There is a puzzle in the issue of the direct effect. In the experiments on ion beam induction of mutation, normally plant seeds with embryos are ion-bombarded. Here, energetic ions must travel through the materials that cover DNA in the cell nucleus before they can directly interact with DNA. Theoretical calculation estimates that the most of the ion energy is lost before the ion can impact with DNA for 30-keV nitrogen ions to pass through organic materials of a-few-hundred nanometers. Questions raised then include whether and how the ultra-low-energy ions are still able to cause DNA damage to induce mutation. Along with experimental efforts, in which keV ions bombarded naked DNA in vacuum and DNA strand breaks and mutation induction were discovered [3–9], molecular simulation is of necessity in studying the interaction between ions even at ultra low energy and DNA at the molecular level to reveal the nature of the interaction. There have been a plenty of studies on ion interaction with solids [10,11] and high-energy radiobiology [12]. However, there are yet lacks of studies on low-energy ion interaction with biological organisms and particularly DNA.

It has been found from experiments that treatments of ion beam on biological matter do not give complete random results, but rather biased ones [13]. For example, in an experiment, the plasmid M_{13}mp18 with the *lacZ* gene was bombarded by N-ion and transferred into host bacteria JM103 *E. coli*. The results revealed that the dominant type of mutation was from a replacement (95%) while the rest was from the base deletion [14], but no insertion or replication of bases was detected. In addition, it was found that cytosine was the most sensitive residue taking more than 50% of the mutations. Another study using C-ion radiation [15] showed different non-random results with one base-deletions taking 38.5%

* Corresponding author. Tel.: +66 5394 3341; fax: +66 5389 2277.
E-mail address: vannajan@gmail.com (V.S. Lee).

1093-3263/$ – see front matter © 2009 Elsevier Inc. All rights reserved.
doi:10.1016/j.jmgm.2009.11.009

of mutations. A comparative study reported a different outcome between N-ion and ^{60}Co-γ ray treated *E. coli* containing *rpoB* genes [16]. It was found that CG-to-TA, AT-to-GC and AT-to-TA took majority in the substitution mutations (92.13% or 82/89) in ^{60}Co-γ radiation, while N-ion bombardment gave CG-to-TA and AT-to-TA as the major substitutions. Moreover, GC-to-CG and AT-to-GC were found induced by N-ion bombardment only but not by the γ-ray, whereas AT-to-CG was not found after N-ion implantation, but was only found in ^{60}Co-γ radiation.

From the above studies, it is clear that there are many distinct molecular mechanisms for radiation-induced mutation which can effect the possible mutations generated from a given mutation method. Ideally to be able to predict and controls of the amount and type of mutation generated by a given method further insight into the mechanisms controlling the processing of mutated DNA is required. Currently, very little knowledge about the molecular mechanisms or pathways of DNA damage during ion beam implantation or other types of radiations has been found [2,15]. To complement the small amount of experimental evidence, some researchers have attempted to use computational methods to investigate the irradiation of DNA. Such studies include simulating accurate structures of mini-circle and super-coiled DNA molecules [19–22], DNA movements [23,24], tracking simulations of radiation particles in DNA molecules [3,25–27] and quantum molecular calculations of DNA damaged by radiation [28,29]. However, no such work has been done with ion beams induced mutation.

In this study, molecular modeling methods were selected to investigate the molecular interactions and elementary processes of DNA during irradiation by ion beam. To complement the experiment work done with N^+ ion beam irradiation, we chose this form of ion beam particles to examine computationally. The study was divided into two main parts: (*i*) a Monte Carlo (MC) simulation of N^+ on a DNA strand and (*ii*) a molecular dynamics (MD) simulation of the effect of N^+ implantation on a DNA strand. The MC simulations aimed to specify the preferred sites of N^+ implantation around an arbitrary short strand of DNA using commercial software packages. The MD simulation aimed to investigate possible changes in the structure of the same DNA molecules after the bombardment. In both parts of the experiment, the DNA was in the A-form to best resemble real world experimental conditions, in which naked solid state DNA samples were bombarded by ion beam under vacuum [9]. Predominantly, this study focused on low-energy ion irradiation, because high-energy (above 10^2 keV) ion irradiation can cause very strong interactions with the DNA structure resulting in extensive damage to the DNA. By focusing our investigation on low-energy ion irradiation, the interaction of ions on DNA molecular sites allows identifying details of the effect of ion interactions to DNA structural changes.

2. Methods

2.1. DNA preparation

A 30-base-pair-long DNA duplex with sequence 5′-AAGAATG-GAA TCAAAGTTAA CTTCAAAATT-3′ was constructed in A-form which was the form commonly observed in the dehydrated samples of DNA under vacuum condition with a pressure of 10^{-4} Pa for ion-bombardment experiments on the glass surface as well as in crystallographic experiments. The selected residues numbered between 760 and 789 bps of the green fluorescent protein plasmid (pGFP) from GenBank, sequenced by Chalfie et al. [30]. This portion of DNA contained the sequence that translates into the flourophore of the functioning protein (green fluorescent protein, GFP). The DNA duplex was built in Discovery Studio 1.7.1 software [31]. The CHARMm27 force field [32] was applied on this molecule. To obtain the DNA structure in the equilibrium state in vacuum, DNA was neutralized with Na-ion. The energy minimization, heating, equilibration and production MD simulation were performed using the Standard Dynamic Cascade protocol. The steps of energy minimization were divided into two parts: 1000 steps of the steepest descent minimization, and 4000 steps of the adopted bases Newton–Raphson minimization. Afterwards, heating was performed for 60 ps from 0.0 to 323.0 K according to the experimental temperature. Then, the equilibration was performed for 2900 ps at 323.0 K. And finally, the production was performed for 40 ps at the same constant temperature. All processes were done in NPT ensemble with the total simulation time of 3 ns. The final DNA structure from the MD simulation was used as the substrate for the adsorption of N^+.

2.2. Monte Carlo simulations of N^+ around a DNA strand

In Materials Studio 4.3 [33], the minimized DNA structure was imported, and the N^+ ion was constructed. The COMPASS force field [34,35] was assigned to both DNA and ion. Then, the adsorption calculations using the Adsorption Locator module were performed for ion fluences of 18 and 27 ions on one DNA molecule (corresponding to 6×10^{13} and 9×10^{13} ions/cm^2 as in the ion-bombardment experiment [9], respectively). In the calculation, the simulated annealing algorithm was performed for 5 cycles, with 15,000 MC simulation steps for each cycle as in Supplementary Fig. S1. The initial temperature was 1000 K before cooling down gradually to 323.0 K during the simulations. The simulation searched for the 10 best configurations of adsorption along with their interaction energy.

The starting configuration was adjusted to the current temperature for many iterating steps. Applying the Metropolis Monte Carlo method decided whether to accept or reject the change of N^+ position. The probability to transform from configuration m to n defined as P_{mn} is:

$$P_{mn} = \min\left[1, \exp\left\{\frac{E_n - E_m}{k_B T}\right\}\right] \quad (1)$$

where k is the Boltzmann constant and T is the simulation temperature [36]. The total energy of configuration m (E_m) is calculated by the following sum:

$$E_m = E_m^{AA} + E_m^{AS} \quad (2)$$

where E_m^{AA} is the intermolecular energy between the adsorbate molecules (N^+) and E_m^{AS} is the interaction energy between the adsorbate molecules and the substrate (DNA) [37].

After the simulations, the results were shown as the equilibrium structure of DNA substrate, radial distribution function (RDF) plots ($g(r)$), distances of maximum RDF (r_{max}) and RDF integrals in the interval of 0.0–4.0 Å ($I_{4Å}$). The RDFs were measured from the N^+ to each of the rest of atom types in the DNA. The atom types were arbitrary defined in the discussion (shown in Fig. 1). The results point out that N^+ ions have specific sites of adsorption preference.

2.3. Molecular dynamics simulations of N^+ ion bombardment of DNA

In Materials Studio, the final structure of the DNA strand adsorbing 27 ions (corresponding to fluence of 9×10^{13} ions/cm^2) with the best interaction energy (the lowest or most negative energy) was used as the initial structure for the simulations of N^+ bombardments. All the nitrogen ion residues were deleted except for the one in the middle of the DNA strand as shown in Fig. 2a. The ion was moved 10 Å further from the strand by editing its Cartesian coordinate in the program database (PDB) file. The classical MD

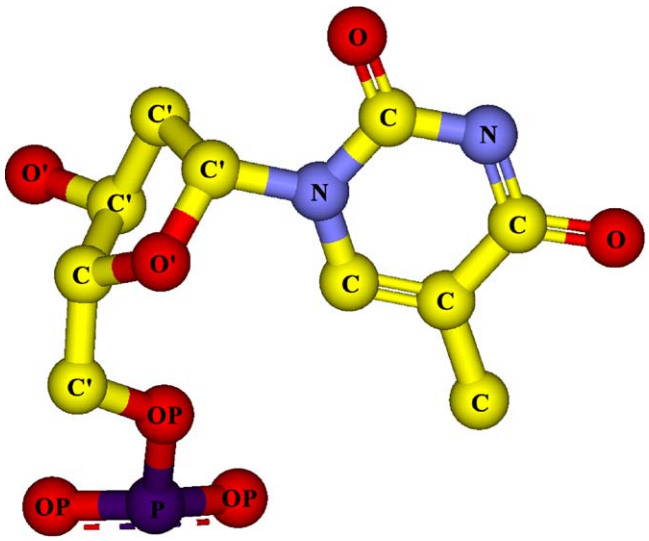

Fig. 1. Atom type definition of the nucleotide. For clear illustration of the MDs constructed DNA, the neutralization is not shown.

simulations of NPT (N: number of atoms, P: pressure, and T: temperature) ensembles at 323 K and 0 atm were performed for bombardments with energy of 0.1, 1, 10, and 100 eV in AMBER 9 [38]. The forcefields for DNA had partial charges explicitly parameterized for solution conditions, and thus might require modification for a vacuum condition. From the previous study by Rueda et al. [38,39], the charges of nucleobases in vacuo were scaled by a factor of 0.8 and the calculations showed that the changes in forcefield parameters had little effect in the conformational transition of the DNA duplex. The time step was 1 fs. The non-bonded cutoff was 9.0 Å. The residues 1–8, 22–38 and 52–60 at the end chains were held fixed. The velocity vectors applied in AMBER were calculated from the ion energy (E) and mass (m) using the equation:

$$v = \left(\frac{E}{2m}\right)^{1/2} \tag{3}$$

where v is the magnitude of the velocity (scalar quantity) and the unit vector for velocity direction was specified as well. The directions of the velocities were assumed to be in the direction from the ion to an arbitrary target atom in DNA calculated using the known coordinate of N^+ and the target atom.

3. Results and discussion

3.1. Ion and DNA interaction

From the energy report calculated by Adsorption Locator shown in Table 1, it was found that the best configuration of the DNA molecule adsorbing 27 N^+ ions had the interaction energy of −26.19 kcal/mol, which was 4.38 kcal/mol lower than the interaction energy of the one adsorbing 18 N^+ ions. The negative values of both fluences indicated that the adsorptions of N^+ on DNA molecules were thermodynamically favorable. The lower (more negative) interaction energy of the DNA molecule adsorbing 27 N^+ points out that the 18 N^+ does not fill the DNA molecule's adsorption capacity since it releases even more energy when adsorbing an extra 9 ions. Moreover, it could be said that the adsorption capacity for the molecule was at least equal to 27 ions, or experimentally, 9×10^{13} ions/cm^2. According to the experiment result reported earlier [9], when the ion fluence increases, the amount of DNA in the supercoiled form decreases and the amount in the linear form increases for N-ion bombardment. This indicates that nitrogen ions even with lower energy are effective in producing double strand breaks and thus more than capable of inducing gene mutation.

Table 1
The interaction energies of the best configuration for each ion fluence.

Ion beam fluence ($\times 10^{13}$ ions/cm^2)	Equivalent number of N^+	Interaction energy (kcal/mol)
6	18	−21.810
9	27	−26.192

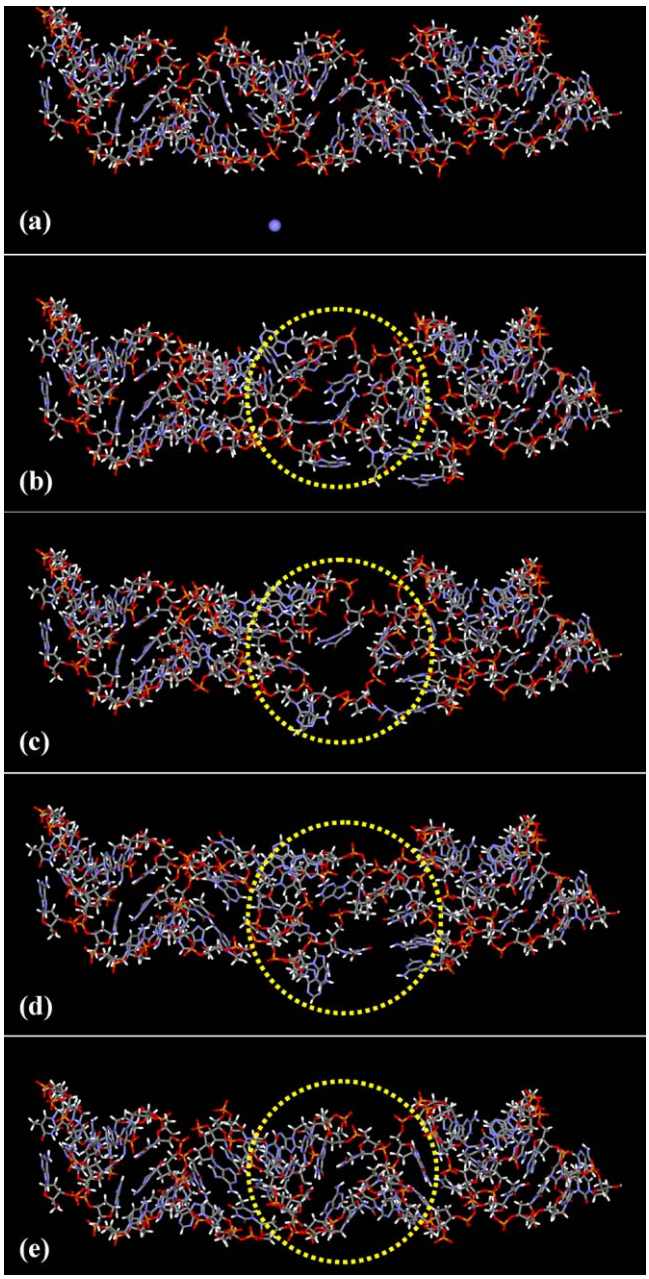

Fig. 2. The initial structure of DNA and the structures after bombardment with varied N-ion energy from selected simulation snapshots. (a) Initial structure; the particle at the low part represents the incident ion. (b) 0.1 eV at 4 ps. (c) 1 eV at 4 ps. (d) 10 eV at 4 ps. (e) 100 eV at 1 ps. The dash-circled areas are the main ion-bombardment-induced change parts.

3.2. Radial distribution functions

Specific sites adsorption preference of N^+ ions interacting with DNA from simulation was detailed. Table 2 summarizes the values

Table 2
Summary of the distance of maximum radial distribution functions, r_{max}, and the integral of radial distribution functions from 0.0 to 4.0 Å, $I_{4Å}$, of each atom type.

Fluence ($\times 10^{13}$ ions/cm^2)	Atom type	r_{max} (Å)	$I_{4Å}$
6	N	4.15	1.77
	O	6.25	1.46
	O′	5.15	1.48
	OP	3.25	3.20
	C	3.95	1.65
	C′	4.05	0.96
9	N	3.55	1.89
	O	3.25	4.15
	O′	3.75	3.73
	OP	3.35	3.30
	C	3.85	1.34
	C′	3.95	1.90

of r_{max} and $I_{4Å}$ for the best configuration at each fluence level. This table shows that, for fluence values equal to 6×10^{13} ions/cm^2, OP (O in phosphate) has the highest RDF integral value of 3.20, approximately twice as large as other cases. This pointed a fact that N^+ preferred to be adsorbed at OP sites in phosphate groups of DNA. A straightforward explanation can be made from the basic chemical knowledge that oxygen atoms in phosphates have negative charge, which can bind strongly with positively charged species by electrostatic interaction. The distances of maximum radial distribution functions, r_{max}, also give similar results. OPs are suggested to have the strongest interaction with N^+, as they have the least r_{max} while other atom types give far greater r_{max} values.

Different results were observed for the fluence of 9×10^{13} ions/cm^2. Here, the three highest RDF integral values were all from oxygen atoms: O (O in bases), O′ (O in sugars) and OP. The integral values for the three atom types were 4.15, 3.73 and 3.28, respectively. This might be because a larger number of ions increase the chance of interacting with other oxygen sites. Hence, oxygen is still the atom of preference for N^+ irradiation. Other atom types give considerably smaller integral values. For this fluence, the values of r_{max} do not show as large differences as found with the previous fluence value. This might also be because of the more ions and thus the more chances to interact with other atoms. Still, oxygen atoms gave smaller value of r_{max} (3.25, 3.75 and 3.35 for O, O′ and OP respectively) compared with those of other atom types (3.55, 3.85 and 3.95 for N, C and C′, respectively). The results also agreed with the fact that oxygen atoms have large electronegativity, a measure of the ability of an atom to attract electrons it is sharing with another, and usually strongly polarize the formed bonds. Therefore, bonds with oxygen atoms are negative dipoles with partially negative charge on the oxygen side and thus they can still attract positively charged species. The RDF plots with the r_{max} reported in Table 2 indicate that N^+ ions are likely to interact with OP, C, C′, N, O′ and O, respectively. The radial distribution function of N^+ around OP in phosphates with a) the fluence of 6×10^{13} ions/cm^2 and b) the fluence of 9×10^{13} ions/cm^2 was provided in Supplementary Fig. S2.

3.3. Molecular dynamic simulations

Our study used molecular dynamics to monitor the change in bond lengths within the DNA as the biomolecule was subjected to ion bombardment, and observed enormous changes in the bond length as described below. Large bond length changes might lead to bond breakage. However, the breakage of covalent bonds cannot be accounted from the simulation due to the limitation of classical MD. A quantum mechanics approach would be a solution for such simulation; however, it requires very small DNA duplexes in the simulation and also some approximations as well. Another limitation of our approach as already mentioned in the method section resides in the forcefield for DNA, in which its partial charges parameterized for solution conditions may not be suitable in vacuo. Nevertheless, molecular dynamics techniques allow detailed time and space resolution for carefully selected systems which could provide details of the structural change in DNA after ion bombardment. The root mean square deviations (RMSD) were collected for every time step of the simulations to study the overall movement of the DNA structures during the simulation. The initial structure of DNA and the structures after bombardment with varied N-ion energy of 0.1, 1, 10, and 100 eV from selected simulation were snapshotted as shown in Fig. 2. At the simulation time of 4 ps, it is clearly seen large structural changes (Fig. 2b–d) in DNA for 0.1, 1, and 10 eV N-ion bombardment. For the highest ion energy of 100 eV, the ion seems to pass through DNA too quickly to snapshot for the change in the DNA structure and the structure even at 1 ps as illustrated in Fig. 2e does not show change compared with the initial structure shown in Fig. 2a. From the RMSD plots in Fig. 3, all bombardments exhibited rapid changes in RMSD during the simulations whereas the RMSDs for the unbombarded system at 298 and 323 K were smaller. At 100 eV ion bombardments, the RMSD peaked after 1.5 ps. Since large RMSD values represent a large movement and flexibility of the DNA structure, it is suggested that the flexibility might result in the simultaneous breakages of chemical bonds in DNA. The upcoming sections will present the changes in each type of bond lengths after the rapid changes in the RMSD.

The ranges and medians of the bond lengths of eight bond types were studied. The studied types included oxygen–phosphorus single bonds (O–P), oxygen–phosphorus aromatic bonds (O–P *(ar)*), carbon–carbon single bonds (C–C), carbon–nitrogen single bond (C–N), carbon–oxygen single bonds (C–O), carbon–carbon aromatic bonds (C–C *(ar)*), carbon–nitrogen aromatic bonds (C–N *(ar)*) and carbon–oxygen double bonds (C=O). The maximum, minimum and modal bond lengths in each bombardment were measured and reported in Tables 3–5. Relative deviations from the equilibrium lengths were noted in the parentheses on the right of the measured bond lengths. The results for the 100 eV bombardments were not presented because the simulation lasted for too short a time to notice bond length changes.

From the tables, the maximum bond lengths of all types were far higher than the equilibrium lengths for all bombardments. The bombardment producing the largest maximum bond lengths was the one with the 1 eV ion beam, followed by ones with 0.1 eV and 10 eV ion beams respectively. This indicates that the energy of 1 eV can cause the most stretching to all the bonds. In the same manner, the bombardment resulting in the largest minimum bond lengths

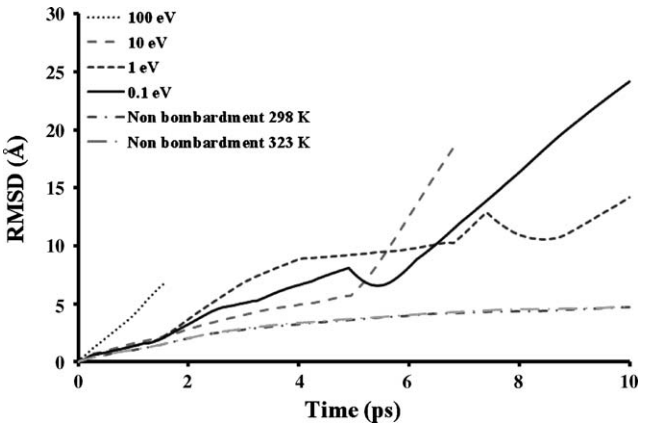

Fig. 3. RMSD plots for the MD simulations of ion bombardments at different ion energies in comparison with the unbombarded systems at 298 and 323 K.

Table 3
Bond length maxima, minima and modes after 10 ps of 0.1 eV bombardment simulations.

Bond type	Average equilibrium length (Å)	Bond length after 0.1 eV bombardment (Å)					
		Maximum		Minimum		Mode	
O–P	1.582	1.817	(+15%)	1.411	(−11%)	1.618	(+3%)
O–P *(ar)*	1.486	1.606	(+8%)	1.306	(−12%)	1.498	(+1%)
C–C	1.518	1.800	(+19%)	1.398	(−8%)	1.560	(+3%)
C–N	1.490	1.664	(+12%)	1.405	(−6%)	1.489	(−0%)
C–O	1.433	1.566	(+9%)	1.302	(−9%)	1.445	(+1%)
C–C *(ar)*	1.387	1.557	(+12%)	1.329	(−4%)	1.426	(+3%)
C–N *(ar)*	1.351	1.604	(+19%)	1.088	(−19%)	1.388	(+3%)
C=O	1.230	1.528	(+24%)	1.133	(−8%)	1.220	(−1%)

Table 4
Bond length maxima, minima and modes after 10 ps of 1 eV bombardment simulations.

Bond type	Average equilibrium length (Å)	Bond length after 1 eV bombardment (Å)					
		Maximum		Minimum		Mode	
O–P	1.582	2.838	(+80%)	1.382	(−13%)	1.702	(+8%)
O–P *(ar)*	1.486	2.236	(+50%)	0.971	(−35%)	1.498	(+1%)
C–C	1.518	2.409	(+58%)	0.939	(−38%)	1.570	(+3%)
C–N	1.490	2.153	(+44%)	1.398	(−6%)	1.543	(+4%)
C–O	1.433	2.373	(+66%)	0.829	(−42%)	1.432	(−0%)
C–C *(ar)*	1.387	2.116	(+53%)	1.116	(−20%)	1.408	(+2%)
C–N *(ar)*	1.351	2.097	(+55%)	0.745	(−45%)	1.381	(+2%)
C=O	1.230	1.787	(+45%)	0.958	(−22%)	1.221	(−0%)

Table 5
Bond length maxima, minima and modes after 6 ps of 10 eV bombardment simulations.

Bond type	Average equilibrium length (Å)	Bond length after 10 eV bombardment (Å)					
		Maximum		Minimum		Mode	
O–P	1.582	1.909	(+21%)	1.471	(−7%)	1.698	(+7%)
O–P *(ar)*	1.486	1.798	(+21%)	1.271	(−14%)	1.481	(−0%)
C–C	1.518	1.702	(+12%)	1.304	(−14%)	1.544	(+2%)
C–N	1.490	1.618	(+9%)	1.396	(−6%)	1.515	(+2%)
C–O	1.433	1.713	(+20%)	1.223	(−15%)	1.459	(+2%)
C–C *(ar)*	1.387	1.648	(+19%)	1.310	(−6%)	1.399	(+1%)
C–N *(ar)*	1.351	1.548	(+15%)	1.145	(−15%)	1.336	(−1%)
C=O	1.230	1.319	(+7%)	1.054	(−14%)	1.218	(−1%)

is still the one with 1 eV ion beam, followed by ones with 10 and 0.1 eV ion beam respectively. It is suggested that this energy gives the strongest shrinkage in overall bonds lengths. However, the bond lengths for 10 eV bombardments were measured at 6 ps since the simulation halted after that. So, the bond lengths due to this bombardment could be further elongated, and, by a rough approximation, the bond lengths could be close to ones bombarded if the simulation had lasted as long as 10 ps.

It was found that the bond type most sensitive to the ion bombardments was the O–P bonds. The maximum and modal lengths of this bond type had the largest deviation amongst all bond types, especially in 1 eV bombardment, where the bonds could elongate to as long as 2.838 Å (80% stretched from the equilibrium length). This corresponds to very large changes in overall RMSDs since the O–P bonds are a part of the DNA backbones. The DNA double helix could have an extreme stretching to twice of its normal length before its base pairs break, demonstrated by both theoretical modeling and nanomanipulation experiments [40]. As the DNA double helix is a multiply bonded structure, a nearly 100% stretching of the bond such as the one obtained above might cause breakage which can affect the overall structures and movements of DNA.

For further analysis of the bond lengths, the relative number of the elongated bonds for each type was recorded in order to study the changes of the bond lengths with changes of time. The percentages of the elongated bonds in DNA during the simulation of each bombardment were reported as line curves in Fig. 4. The percentage is calculated by dividing the counts of the elongated bonds (the bonds with more than 5% elongation) by the total counts of the bonds of the specific type. For example, if the total count of the O–P in the structure is 116, and the count of elongated O–P is 20, then the percent of the elongated bonds for the O–P in this structure is calculated as 20/116 = 17.2%.

From the figures, it was found that most of the bonds in the DNA tended to be elongated as time went by. This could be seen in the rising curves throughout the simulations. Some of the curves (especially for 0.1 eV bombardments) declined during some periods because the criterion of 5% elongation might still be too small for bond breakages. Furthermore, the three bond types with the largest percentage of the elongated bonds were O–P, C–C and C–C *(ar)* (navy, scarlet and orange graphs, respectively). And, the two types with the least percent of the elongated bonds were O–P *(ar)* and C=O (magenta and blue graphs respectively). So, major breakages would most probably occur in O–P, C–C and C–C *(ar)* as

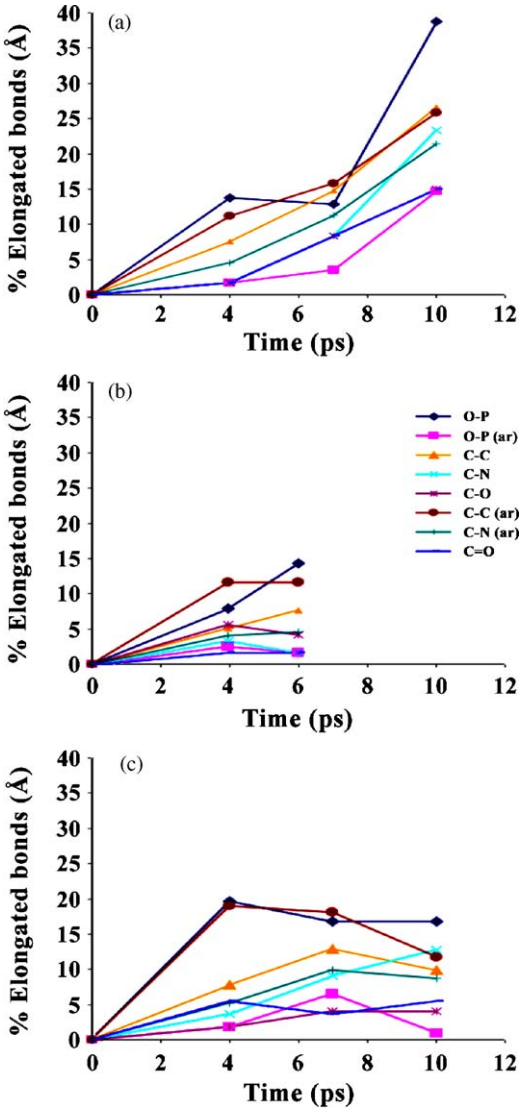

Fig. 4. Percentages of the elongated bonds in DNA during the simulation of (a) 10 eV, (b) 1 eV, and (c) 0.1 eV bombardments.

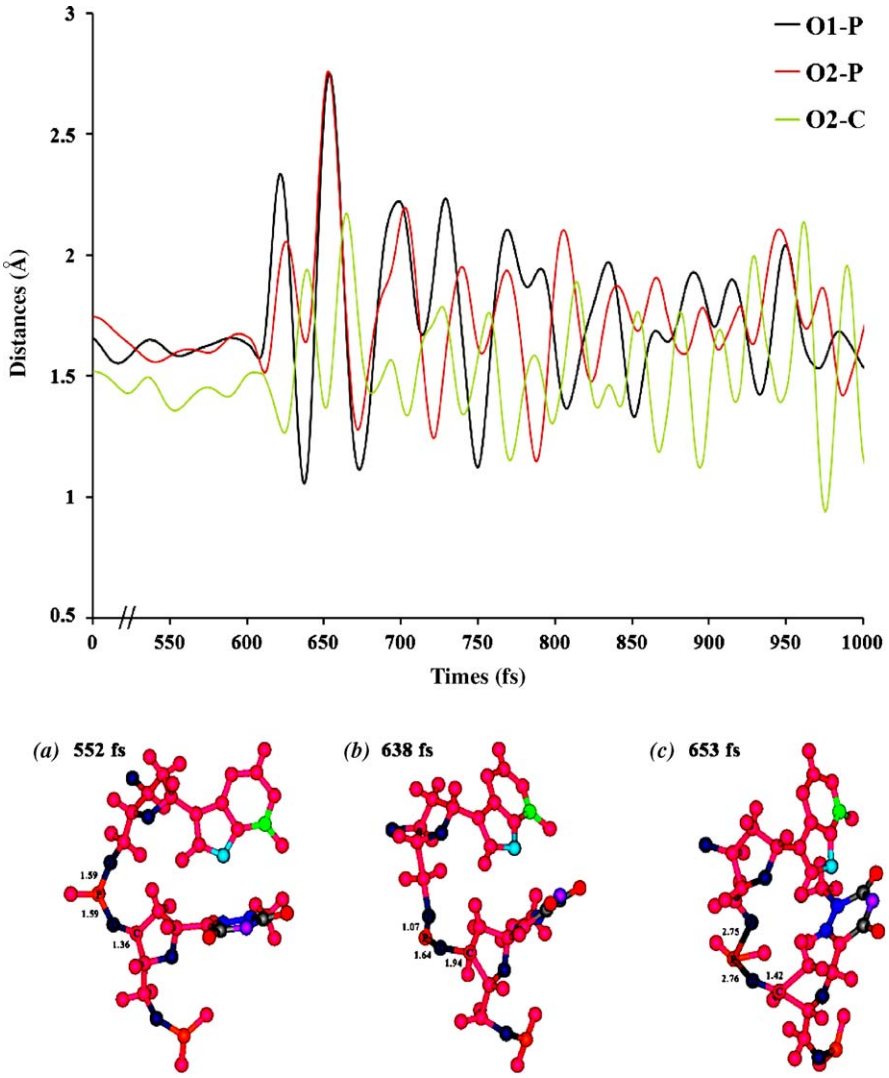

Fig. 5. Demonstration of the elongate distances of O1-P, O2-P, and O2-C as a function of time during 1 eV N-ion bombardment of DNA. At the lower part are the pictures of the structure (O1-P, O2-P and O2-C) selected at time of 552, 638, and 653 fs, respectively.

the DNA was bombarded, thus causing DNA damage. The elongate distances between O1-P, O2-P, and O2-C were observed during the first 1-ps trajectory of 1-eV N-ion bombardment of DNA as demonstrated in Fig. 5. The large displacement was started at 638 fs when the N-ion impacted on the DNA. The selected structure at 552, 638, and 653 fs showed the dynamics of the three breakable bonds at O1-P, O2-P and O2-C. From the usual thermal fluctuations, O–P and O–C fluctuation of the unbombarded system showed low RMSD below 0.5 at 298 and 323 K (the data is not shown). The counter ions were not included in the figure since they were distributed in other locations. The observation agrees well with the RMSD results shown in Fig. 3, which corresponded to rapid changes in the structures after ion bombardment in comparison with the lower RMSD observed in the unbombarded system at 298 and 323 K. The graphs of the bond lengths also showed sudden changes at a corresponding time (7–10 ps). This can be explained that if breakages occurred in the DNA molecule, the molecular structure would have more freedom to move. On the other hand, for the 10 eV bombardments, Fig. 3 shows a correspondence of the graphs with the RMSD only for O–P. In contrast, the 0.1 bombardment did not show such a correspondence.

When comparing the energies of ion bombardments with the mean bond enthalpies (normally a few hundreds to no more than a thousand kcal/mol) [30], we found that most of the mean bond enthalpies were in the range of the energies of bombardments (0.1–10 eV corresponding to the energy range of 10–932 kJ/mol). The relevance of the ranges indicated the sensibility of the simulations.

4. Conclusion

Ultra-low-energy ion bombardment of DNA in vacuum condition was simulated with the example of 0.1–100 eV nitrogen ions to study effects of the ion-DNA interaction on DNA damage. Monte Carlo simulations of adsorption of N^+ on DNA revealed some information of interactions of N^+ with DNA. The fluence of 9×10^{13} ions/cm^2 due to its lower interaction energy with DNA resulted in stronger adsorption of N^+ on DNA molecule than the fluence of 6×10^{13} ions/cm^2. From the RDF analysis, N^+ ions are likely to interact with OP, C, C′, N, O′, and O site in DNA. MD simulations of the N^+ bombardment on DNA molecules exhibited some interesting behavior of the DNA after collisions with N^+. Firstly, the RMSDs of the DNA bombarded by N^+ showed rapid increases after collisions. This might be due to the stretching and then probable breakage of bonds in the structures leaving the molecules more flexible. Further investigation of the stretching bonds was also studied using bond length analysis. The analysis of the bond length maxima, minima and modes showed that all types of bonds had stretching and shrinkage after the bombardment. Additionally, the

modes also gave the same tendency. The bombardment energy of 1 eV resulted in the most extreme maxima and minima, as well as the largest values of the modes of the bond lengths. The analysis also pointed out that the O–P bonds were the most sensitive to the collision. Lastly, the bond length changes with time for each bombardment were also studied. The O–P, C–C and C–C *(ar)* were the most vulnerable bonds in the DNA strands to ion bombardment. The bond enthalpies of these bond types corresponded well with the applied energy.

Acknowledgements

This research was supported by the Institute of Promotion of Science and Technology Teaching (IPST), the Thailand Research Fund (TRF), the Center for Innovation in Chemistry (PERCH-CIC), and the Thailand Center of Excellence in Physics (ThEP). The software resource is the courtesy of National Nanotechnology Center (NANOTEC), Thailand.

Appendix A. Supplementary data

Supplementary data associated with this article can be found, in the online version, at doi:10.1016/j.jmgm.2009.11.009.

References

[1] L.D. Yu, T. Vilaithong, I. Brown, Introduction to Ion Beam Biotechnology. English edition, originally authored by Yu Zengliang in Chinese, Springer Science & Business Media, New York, 2006.
[2] Z. Wei, H. Xei, G. Han, Nucl. Instrum. Methods B95 (1994) 371.
[3] Y. Zhao, Z. Tan, G.Y. Qiu, Y.H. Du, Nucl. Instrum. Methods B211 (2003) 211.
[4] C.A. Hunniford, D.J. Timson, R.J.H. Davies, R.W. McCullough, Phys. Med. Biol. 52 (2007) 3729.
[5] Y. Chen, B. Jiang, X. Ding, X. Liu, C. Chen, X. Guo, G. Yin, Radiat. Environ. Biophys. 37 (1998) 101.
[6] S. Lacomb, Sech C. Le, V.A. Esaulov, Phys. Med. Biol. 49 (2004) N65.
[7] Z.W. Deng, I. Bald, E. Illenberger, M.A. Huels, Phys. Rev. Lett. 95 (2005) 153201.
[8] F.A. Chacon, Ion induced radiation damage on the molecular level, Ph.D. Thesis, University of Groningen, 2007.
[9] R. Norarat, N. Semsang, S. Anuntalabhochai, L.D. Yu, Very low-energy and low-fluence ion beam bombardment of naked plasmid DNA, Nucl. Instrum. Methods B 267 (2009) 1650–1653.
[10] H. Ryssel, I. Ruge, Ion Implantation, Wiley Chichester, 1996.
[11] M. Nastasi, J.W. Mayer, J. Hirvonen, Ion-Solid Interactions: Fundamentals and Applications, Cambridge University Press, 1996.
[12] E. Hall, Radiobiology for Radiobiologists, Lippincott Williams & Wilkins, 1993.
[13] Z. Yu, Study on the interaction of low-energy ions with organisms, Surf. Coat. Technol. 201 (2007) 8006–8013.
[14] J. Yang, L. Wu, L. Li, et al., Sequence analysis of lacZ? mutations induced by ion beam irradiation in double-stranded $M_{13}mp_{18}$ DNA, Sci. China C. Life. Sci. 40 (1997) 107–112.
[15] Q. Wang, G. Zhang, Y.H. Du, Y. Zhao, G.Y. Qiu, Low-energy (30 keV) carbon ion induced mutation spectrum in the lacZ gene of M13mp18 double-stranded DNA, Mutat. Res. Fundam. Mol. Mech. Mutagen. 528 (2003) 55–60.
[16] C.X. Xie, A. Xu, L.J. Wu, et al., Comparison of base substitutions in response to nitrogen ion implantation and ^{60}CO-γ ray irradiation in *Escherichia coli*, Genet. Mol. Biol. 27 (2004) 284–290.
[19] E.A. Kummerle, E. Pomplun, A computer-generated supercoiled model of the pUC19 plasmid, Eur. Biophys. J. 34 (2005) 13–18.
[20] C. Bouchiat, M. Mezard, Elastic rod model of a supercoiled DNA molecule, Eur. Phys. J. E. 2 (2000) 377–402.
[21] F. Lankas, R. Lavery, J.H. Maddocks, Kinking occurs during molecular dynamics simulations of small DNA minicircles, Structure 14 (2006) 1527–1534.
[22] W.K. Olson, V.B. Zhurkin, Modeling DNA deformations, Curr. Opin. Struct. Biol. 10 (2000) 286–297.
[23] L.J. Maher, Mechanisms of DNA bending, Curr. Opin. Struct. Biol. 2 (1998) 688–694.
[24] H. Nikjoo, C.E. Bolton, R. Watanabe, et al., Modelling of DNA damage induced by energetic electrons (100 eV to 100 keV), Radiat. Prot. Dosimetry 99 (2002) 77–80.
[25] H. Nikjoo, D. Emfietzoglou, R. Watanabe, S. Uehara, Can Monte Carlo track structure codes reveal reaction mechanism in DNA damage and improve radiation therapy? Radiat. Phys. Chem. 77 (2008) 1270–1279.
[26] R. Watanabe, H. Nikjoo, Modelling the effect of incorporated halogenated pyrimidine on radiation-induced DNA strand breaks, Int. J. Radiat. Biol. 78 (2002) 953–966.
[27] H. Nikjoo, P. O'Neill, W.E. Wilson, D.T. Goodhead, Computational approach for determining the spectrum of DNA damage induced by ionizing radiation, Radiat. Res. 156 (2001) 577–583.
[28] X. Li, M.D. Sevilla, L. Sanche, Density functional theory studies of electron interaction with DNA: can zero eV electrons induce strand breaks? J. Am. Chem. Soc. 125 (2003) 13668–13669.
[29] J.M. Falcone, D. Becker, M.D. Sevilla, S.G. Swarts, Products of the reactions of the dry and aqueous electron with hydrated DNA: hydrogen and 5,6-dihydropyrimidines, Radiat. Phys. Chem. 72 (2005) 257–264.
[30] M. Chalfie, Y. Tu, G. Euskirchen, W.W. Ward, D.C. Prasher, Green fluorescent protein as a marker for gene expression, Science 263 (1994) 802–805.
[31] Discovery studio 1.7.1, Accelrys Software Inc., San Diego, CA, 2006.
[32] N. Foloppe, A.D. MacKerell Jr., All-atom empirical force field for nucleic acids: I. Parameter optimization based on small molecule and condensed phase macromolecular target data, J. Comput. Chem. 21 (2000) 86–104.
[33] Materials Studio Modeling 4.3, Accelrys Software Inc., San Diego, CA, 2008.
[34] H. Sun, Compass: an ab initio force-field optimized for condensed-phase applications; overview with details on alkane and benzene compounds, J. Phys. Chem. B 102 (1998) 7338–7364.
[35] D. Rigby, H. Sun, B.E. Eichinger, Computer simulations of poly-(ethylene oxide): force field, PVT diagram and cyclization behavior, Polym. Int. 44 (1997) 311–330.
[36] N. Metropolis, A.W. Rosenbluth, M.N. Rosenbluth, A.H. Teller, E. Teller, Equation of state calculations by fast computing machines, J. Chem. Phys. 21 (1953) 1087–1092.
[37] D.A. Case, T.A. Darden, T.E. Cheatham Iii, et al., AMBER 9 (2004).
[38] M. Rueda, S.G. Kalko, F.J. Luque, M. Orozco, The structure and dynamics of DNA in the gas phase, J. Am. Chem. Soc. 125 (2003) 8007–8014.
[39] M. Rueda, F.J. Luque, M. Orozco, Nature of minor-groove binders DNA complexes in the gas phase, J. Am. Chem. Soc. 127 (2005) 11690–11698.
[40] A. Lebrun, R. Lavery, Modelling extreme stretching of DNA, Nucl. Acids Res. 24 (12) (1996) 2260–2267.